

# Introducing the *CSBio II*

Automated Peptide Synthesizer



## We will cover the night shift.

Whether you are tired of manual synthesis, waiting for ordered peptides or want to expand your lab's automated synthesis capabilities, the *CSBio II* is perfect for you. Set up your synthesis in minutes with just a few clicks and return to your finished peptide.

Your time is precious. Let the *CSBio II* maximize what you have.

See the *CSBio II* in action. Visit us at [www.csbio.com/csbioii.html](http://www.csbio.com/csbioii.html) or contact us at [instrument@csbio.com](mailto:instrument@csbio.com) to schedule a virtual demo.

Easy to use

Make your 20 mer in < 5 hours


50 - 500mg of high purity peptide

**CSBi@**  
INSTRUMENTATION



**SPECIAL ISSUE ARTICLE**

# Formulation matters! A spectroscopic and molecular dynamics investigation on the peptide CIGB552 as itself and in its therapeutical formulation

Marco Savioli<sup>1</sup> | Lorenzo Antonelli<sup>1</sup> | Gianfranco Bocchinfuso<sup>1</sup> |  
Francesca Cavalieri<sup>1,4</sup> | Rita Cimino<sup>1</sup> | Emanuela Gatto<sup>1</sup> | Ernesto Placidi<sup>2</sup> |  
Julio Raul Fernandez Masso<sup>3</sup> | Hilda Garay Perez<sup>3</sup> | Hector Santana<sup>3</sup> |  
Maribel Guerra-Vallespi<sup>3</sup> | Mariano Venanzi<sup>1</sup> 

<sup>1</sup>PEPSA-LAB, Department of Chemical Sciences and Technology, University of Rome Tor Vergata, Rome, Italy

<sup>2</sup>Department of Physics, University of Rome 'Sapienza', Rome, Italy

<sup>3</sup>Center for Genetic Engineering and Biotechnology, Havana, Cuba

<sup>4</sup>School of Science, RMIT University, Melbourne, Victoria, Australia

**Correspondence**

Mariano Venanzi, PEPSA-LAB, Department of Chemical Sciences and Technology, University of Rome Tor Vergata, Via della Ricerca Scientifica 1, 00133, Rome, Italy.  
Email: venanzi@uniroma2.it

**Funding information**

H2020 Marie Skłodowska-Curie Actions, Grant/Award Number: 872233

Synthetic therapeutic peptides (STP) are intensively studied as new-generation drugs, characterized by high purity, biocompatibility, selectivity and stereochemical control. However, most of the studies are focussed on the bioactivity of STP without considering how the formulation actually used for therapy administration could alter the physico-chemical properties of the active principle. The aggregation properties of a 20-mer STP (Ac-His-Ala-Arg-Ile-Lys-D-Pro-Thr-Phe-Arg-Arg-D-Leu-Lys-Trp-Lys-Tyr-Lys-Gly-Lys-Phe-Trp-NH<sub>2</sub>), showing antitumor activity, were investigated by optical spectroscopy and atomic force microscopy imaging, as itself (CIGB552) and in its therapeutic formulation (CIGB552TF). It has found that the therapeutic formulation deeply affects the aggregation properties of the investigated peptide and the morphology of the aggregates formed on mica by deposition of CIGB552 and CIGB552TF millimolar solutions. Molecular dynamics simulations studied the first steps of CIGB552 aggregation under physiological ionic strength conditions (NaCl 150 mM), showing that peptide oligomers, from dimers to tetramers, are preferentially formed in this environment. Interestingly, cell viability assays performed on H-460 cell lines indicate a major antiproliferative activity of the peptide in its therapeutic formulation with respect to the peptide aqueous solution.

**KEYWORDS**

atomic force microscopy imaging, fluorescence spectroscopy of peptides, molecular dynamics simulation, peptide aggregation, peptide fibrillation, therapeutic peptide

## 1 | INTRODUCTION

Despite the relevant progress in the prevention and therapy of tumours, cancer diseases remain one of the most important causes of death. Chemotherapy drugs currently in use target quite successfully tumour cells but, unfortunately, are biased by deleterious side effects on healthy cells and tissues. This dramatic situation urges for the search of a new generation of drugs, and those based on synthetic therapeutic

peptides (STP) represent one of the most promising sources.<sup>1</sup> STP possess the distinct advantage of being biocompatible, highly selective, and obtainable with good enantiomeric purity and stereochemical control applying well-established synthetic procedures.<sup>2</sup> Design of new STP aims to optimize their pharmacokinetics in terms of bioavailability, biodegradability and affinity for receptors or target cells.<sup>3,4</sup>

Among the many promising applications for biotherapy, STP have been proposed as potential antitumor agents for their fast diffusion

through biological tissues and enhanced cell permeabilization properties. Furthermore, peptide drugs have shown potent antineoplastic activity interfering with several molecular mechanisms involved in the carcinogenesis, inhibiting angiogenesis or blocking protein-protein interactions.<sup>5</sup> Peptide receptor antagonists featuring pro-apoptosis properties have also been investigated for limiting the growth of tumours.<sup>6</sup>

Recently, a new therapeutic peptide, derived from *Limulus sp.*, and based on the amphipathic cyclic pentapeptide LALF<sub>32-51</sub>, denoted as L2, was investigated as a novel antitumor peptide.<sup>7</sup> With the aim to improve the antitumor activity of L2, some of us from the Center of Genetic Engineering and Biotechnology (CIGB) of Havana (Cuba) synthesized a new linear peptide analogue of L2, denoted in the following as CIGB552.<sup>8</sup> L2 was modified by including a proline (P(6)) and a leucine (L(11)) residues in the peptide sequence as D-amino acids, and an acetyl (Ac) group at the N-terminus.

These modifications were shown to improve the antitumor activity of L2, increasing its apoptosis efficiency and its capacity to inhibit cell proliferation.<sup>8</sup> CIGB552 has also proven to be effective in reducing the size of tumour and increasing lifespan in tumour-bearing mice,<sup>9</sup> and in dogs with naturally-occurring cancer.<sup>10</sup> It has also been found that CIGB552 decreased the microvessel density in the HT-29 xenograft human, suggesting potent anti-angiogenesis properties.<sup>9</sup>

The unique capabilities of CIGB552 arise from its cell-penetrating properties, which allow it to enter cells and elicit a pro-apoptotic effect through its major mediator, the COMMD1 protein,<sup>11,12</sup> a pleiotropic factor involved in the regulation of many cellular and physiological processes that include oxidative stress, protein trafficking, NF- $\kappa$ B-mediated transcription and oncogenesis.

Recently, it has been demonstrated that endocytosis is a preferred mechanism for CIGB552 internalization, which in turn favours the interaction between the peptide and COMMD1 in the endosomal compartment, as proved by proteomics and genomics experiments.<sup>13-15</sup> It has also been shown that the ability of CIGB552 to negatively modulate NF- $\kappa$ B and HIF-1 pathways is impaired in the COMMD1 Knock-out NCI-H460 cell line, confirming that COMMD1 is essential for the peptide mechanism of action.

It should be noted that in the final pharmaceutical formulation, the active substance, currently in clinical phase 2, is administrated

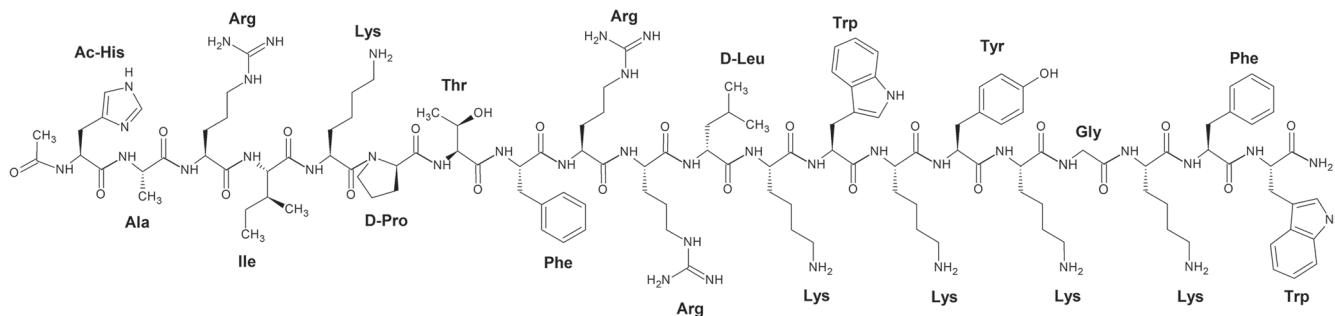
with excipients, that usually do not explicate a direct therapeutic activity, but protects the active substance from chemical effectors and facilitates its pharmacokinetics.

In this work, we compared the physico-chemical properties of CIGB552 in water with those of the same peptide in a formulation mimicking drug administration conditions, containing  $\alpha,\alpha$ -trehalose and (L)-tartaric acid as excipients. The latter system will be denoted in the following as CIGB552TF for brevity, where the suffix TF denotes CIGB552 in its therapeutic formulation. The molecular formula of CIGB552 (Ac-His-Ala-Arg-Ile-Lys-D-Pro-Thr-Phe-Arg-Arg-D-Leu-Lys-Trp-Lys-Tyr-Lys-Gly-Lys-Phe-Trp-NH<sub>2</sub>) is reported in Scheme 1. The presence in the peptide chain of three intrinsically fluorescent residues, that is, W(13), Y(15) and W(20), allowed us to apply optical spectroscopy techniques to characterize the aggregation process of CIGB552 in water and in the therapeutic formulation. Atomic force microscopy (AFM) imaging experiments and Molecular Dynamics (MD) simulations were also carried out to investigate on the morphology of the aggregates and on the structure of both the isolated peptide and the small peptide clusters nucleating the growth of large peptide aggregates, respectively.

## 2 | MATERIALS AND METHODS

### 2.1 | Materials

CIGB552 was synthesized at the Center for Genetic Engineering and Biotechnology (Havana, Cuba). Details of the synthesis has already been reported elsewhere.<sup>9</sup> Briefly, CIGB552 was obtained by solid-state synthesis using the Fmoc strategy, and purified by RP-HPLC inverse (purity >95%) under an acetonitrile/trifluoroacetic acid gradient. The peptide was characterized by electrospray mass spectrometry (Micromass, UK) and NMR spectroscopy. A CIGB552 formulation (CIGB552TF), containing 32.1% (w/w) CIGB552, 50.7%  $\alpha,\alpha$ -trehalose, and 17.2% (L)-tartaric acid, was also prepared for mimicking drug administration conditions. All the solutions for spectroscopy and microscopy experiments were prepared from a 0.28 mM peptide stock solution at pH 7.2.



**SCHEME 1** Molecular formula of the therapeutic peptide investigated (CIGB552)

## 2.2 | Spectroscopy

UV-Vis absorption measurements were carried out at room temperature by a Cary100 Scan spectrophotometer, using  $3 \times 3$ -mm quartz cuvettes (Hellma). Steady-state fluorescence measurements were carried out by a Fluoromax-4 (HORIBA, Jobin Yvon), using a  $3 \times 3$ -mm quartz cuvette at room temperature. Fluorescence emission and excitation spectra were measured at the excitation wavelengths of 280 and 295 nm and emission wavelengths of 360 and 420 nm, respectively.

Circular dichroism (CD) spectra were collected from 190 to 250 nm with a JASCO J-1500 (JASCO-Europe Corporation, Italy) instrument, equipped with a thermostated cell holder set at 25°C, and purged with ultra-pure nitrogen gas. For each sample the spectra were accumulated 8 times (scan speed: 20 nm/min, bandwidth 2 nm; sensitivity: 20 mdeg). The samples were dissolved in high purity water (Milli-Q) extracted from a Millipore system with resistivity of 18.2 M $\Omega$ /cm at 25°C at different concentrations. CD spectra of CIGB552TF were subtracted by the spectra of the excipients (placebo solution of  $\alpha,\alpha$ -trehalose and L-tartaric acid) measured under the same experimental conditions and concentrations. Secondary structure analysis was carried out using the code BeSTSel, freely available at <https://bestsel.elte.hu>.<sup>16</sup>

## 2.3 | Atomic force microscopy

AFM experiments were carried out in air at room temperature on a Veeco Multiprobe IIIa instrument (Santa Barbara, CA). The AFM measurements were carried out in tapping mode on a film obtained by drop casting 1-mM aqueous solutions of CIGB552 or CIGB552TF on mica, and incubating for 18 h in a dryer. For the AFM measurements, a Si super sharp tip, functionalized by carbon flake was used (curvature 1 nm, elastic constant 5 N/m, resonance frequency 150 kHz).

## 2.4 | Molecular dynamics simulations

MD simulations were performed using the GROMACS package version 2019.6<sup>17</sup> with a modified GROMOS96 53a6-FF<sup>18</sup> force field

including parameters for D-Pro and D-Leu residues. In order to analyse the peptide conformational landscape and aggregation properties, MD simulations with 1 and 4 CIGB552 molecules were carried out in 150 mM NaCl aqueous solution (MD1A, MD4A) and in water (MD1B, MD4B) (Table 1). Time steps of 2 fs were used for equilibration and production runs. The equilibrium temperature (300 K) was controlled by velocity rescaling<sup>19</sup> with a coupling constant of 0.1 ps.

To mimic the therapeutic formulation environment, MD simulations were also carried out placing one CIGB552, three (L)-tartaric acid and three  $\alpha,\alpha$ -trehalose molecules in a 411 nm<sup>3</sup> cubic box containing 13328 water molecules (MD1C). Two chloride (Cl<sup>-</sup>) ions were added in order to neutralize the net charge of the system. Initial configurations were randomly generated by *gmx insert-molecules* Gromacs tool. The parameters for the excipients were taken from the Automated Topology Builder server.<sup>20,21</sup>

Pressure was controlled by an isotropic Parrinello-Rahman barostat<sup>22</sup> with a coupling constant of 2 ps and a reference external pressure of 1 atm. Lennard-Jones long range interactions were treated with a cut-off radius of 1.2 nm. Coulombic interactions were calculated by the Particle Mesh Ewald method.<sup>23</sup> 200 ns-long simulations have been performed for three replicas of each system having different starting configurations. MD simulation analyses were carried out using either built-in GROMACS tool and handmade Tcl script in VMD.<sup>24</sup> Relative solvent accessibility (RSA) was calculated as the ratio between the solvent accessibility surface area (SASA) value and the maximum solvent accessible surface area for each residue.<sup>25</sup> Secondary structure content was assessed through the DSSP (Dictionary Secondary Structure of Proteins) algorithm.<sup>26</sup> SASA and gyration radii were used to evaluate the equilibration time of each MD. RMSD-based cluster analysis was carried out applying similarity conditions with a 0.2 nm cut-off.<sup>27</sup> In the case of MD simulations of the therapeutic formulation, a further NVT equilibration step of 100 ps with 1 fs integration time at 10 K with position restraint on the heavy atoms of peptide and excipients was required to obtain the correct equilibration of the system.

## 2.5 | Cell viability assay

Cell viability assay was carried out on the H-460 (ATCC, HTB-117) cell line, maintained at 37 °C and 5% CO<sub>2</sub> in RPMI 1640, and

**TABLE 1** Experimental conditions for MD simulations at  $T = 300$  K with 1 and 4 CIGB552 molecules in 150-mM NaCl aqueous solution (MD1A and MD4A), in water (MD1B, MD4B) and in a (L)-tartaric acid,  $\alpha,\alpha$ -trehalose water solution (MD1C)

MD simulation	Box dimensions (nm) <sup>3</sup>	Number of CIGB552 molecules	Number of water molecules	Number of Na <sup>+</sup> ions	Number of Cl <sup>-</sup> ions
MD1A	5.44 × 5.44 × 5.44	1	5005	15	23
MD1B	5.44 × 5.44 × 5.44	1	5035	—	8
MD1C <sup>a</sup>	7.43 × 7.43 × 7.43	1	13328	—	2
MD4A	4.98 × 4.98 × 7.96	4	5964	18	50
MD4B	4.98 × 4.98 × 7.96	4	5996	—	32

<sup>a</sup>(L)-tartaric acid: 3;  $\alpha,\alpha$ -trehalose: 3.



supplemented with 10% foetal bovine serum (HyClone, Logan, UT) plus 30  $\mu\text{g}/\text{ml}$  of gentamycin (Gibco). Proliferative assay was performed as previously described.<sup>7</sup> Peptide concentrations ranging from 0 to 300  $\mu\text{M}$  were added to 10,000 cells/well and incubated for 48 h at 37 °C in 5%  $\text{CO}_2$ . Subsequently, 50  $\mu\text{l}$  of 80% trichloroacetic acid solution were added to the cells and incubated for one hour at 4 °C. Finally, 100  $\mu\text{l}$  of the sulforhodamine B solution were added to the wells, and absorbance was measured at  $\lambda = 492$  nm. Each sample point was carried out in triplicate, and experiments were performed twice. IC50 values were obtained from the respective growth curves.

### 3 | RESULTS AND DISCUSSION

#### 3.1 | UV-Vis absorption

The absorption spectrum of CIGB522 in the near UV region is determined by the overlap of the  $n \rightarrow \pi^*$  transition of the Trp [ $\lambda_{\text{max}} = 283$  nm;  $\epsilon(283) = 5800 \text{ M}^{-1} \text{ cm}^{-1}$ ] and Tyr residues [ $\lambda_{\text{max}} = 274$  nm;  $\epsilon(274) = 1400 \text{ M}^{-1} \text{ cm}^{-1}$ ] comprised in the peptide sequence. For comparison, the absorption spectra of CIGB522TF in the concentration range between 5.2 and 280  $\mu\text{M}$  are reported in Figure 1A. From these data, we determined the molar extinction coefficient of CIGB522TF at 280 nm [ $\epsilon(280) = 12500 \text{ M}^{-1} \text{ cm}^{-1}$ ], in good agreement with the sum of the molar extinction coefficients of the aromatic

residues reported above. This finding indicates that strong (short-range) ground-state interactions between the aromatic moieties of CIGB522 in its therapeutic formulation can be neglected. It should be noted that the shapes of the absorption spectra of CIGB522 in its therapeutic formulation and in solution are strictly the same (data not shown). On the contrary, while for the former the measured absorbances were found to closely follow the linear trend forecast by the Lambert-Beer law, for the latter a marked deviation from the linear behaviour is observed at the higher concentrations (Figure 1B), suggesting that CIGB522 in water may give rise to the formation of aggregates at micromolar ( $>50 \mu\text{M}$ ) concentrations.

#### 3.2 | Fluorescence

Fluorescence emission spectra of CIGB522 and CIGB522TF were measured at  $\lambda_{\text{ex}} = 280$  (both Tyr and Trp photoexcited) and at  $\lambda_{\text{ex}} = 298$  nm (selective photoexcitation of Trp). For both the excitation wavelengths, the fluorescence emission spectra of CIGB522 in water and in the therapeutic formulation, show a relatively broad emission band centred at  $\lambda_{\text{em}} = 359$  nm, typical of the indole emission in a polar environment (Figure S1). The close similarity of the emission spectra measured at  $\lambda_{\text{exc}} = 280$  and 298 nm indicates that an almost total Tyr  $\rightarrow$  Trp energy transfer takes place for both the CIGB522 formulations.

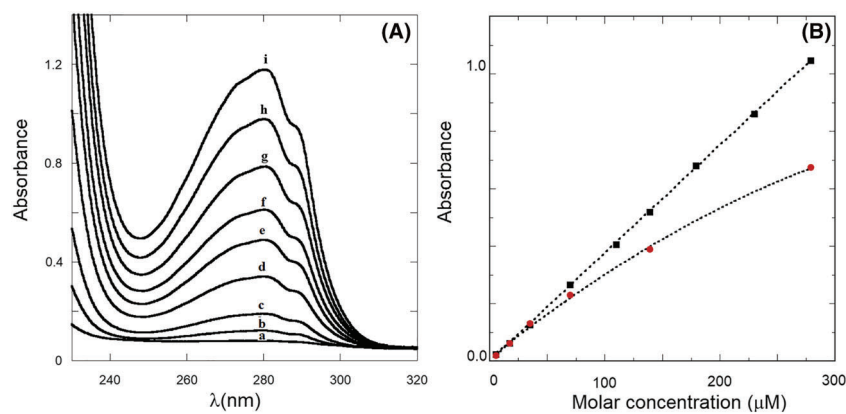


**FIGURE 1** UV absorption experiment on CIGB522. (A) Absorption spectra of CIGB522TF (therapeutic formulation) at different peptide concentrations [(a) 5; (b) 17; (c) 35; (d) 70; (e) 110; (f) 139; (g) 179; (h) 230; (i) 279  $\mu\text{M}$ ]; (B) Absorbance at  $\lambda = 280$  nm for different peptide concentrations (same of Figure 1A). Red dots: CIGB522; black squares: CIGB522TF

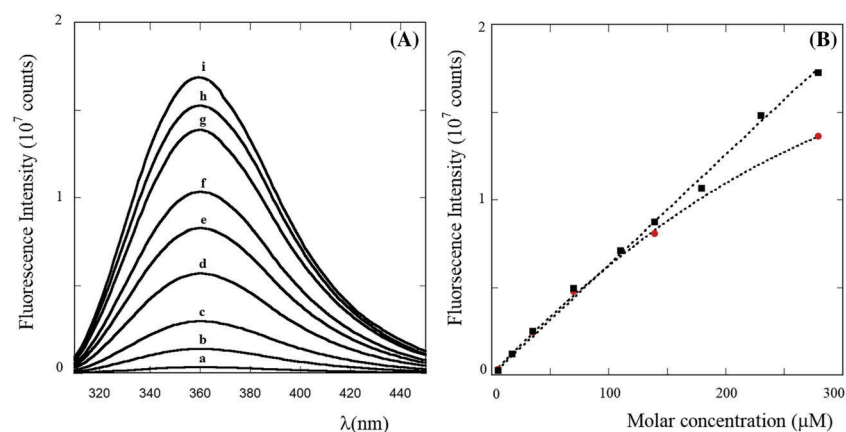


**FIGURE 2** (A) Fluorescence spectra ( $\lambda_{\text{ex}} = 298$  nm) of CIGB522TF (therapeutic formulation) at different peptide concentrations [(a) 5; (b) 17; (c) 35; (d) 70; (e) 110; (f) 139; (g) 179; (h) 230; (i) 279  $\mu\text{M}$ ]. (B) Fluorescence intensity ( $\lambda_{\text{ex}} = 298$  nm;  $\lambda_{\text{em}} = 359$  nm) for different peptide concentrations (same of Figure 2A). Red dots: CIGB522; black squares: CIGB522TF

Emission spectra for different concentrations of CIGB552TF at  $\lambda_{\text{ex}} = 298$  nm are shown in Figure 2A. Where the emission intensities of CIGB552 and CIGB552TF at  $\lambda_{\text{em}} = 359$  nm are reported as a function of the peptide concentration, the same intensity vs. concentration trend observed by UV absorption measurements is obtained. In particular, in the case of CIGB552TF, it has found a linear dependence of the emission intensity on the peptide concentration, while for the higher concentrations (>100  $\mu\text{M}$ ) of the peptide water solutions an asymptotic trend is obtained (Figure 2B). The same trend was observed for  $\lambda_{\text{exc}} = 280$  nm (data not shown). These results, in parallel with the UV absorption findings, strongly suggest that CIGB552, but not CIGB552TF, gives rise to the formation of aggregated species at the higher concentrations investigated.

### 3.3 | Circular dichroism

CD experiments were carried out for different micromolar concentrations of CIGB552 in water solution and in the therapeutic formulation. From the CD spectra, characterized by a single minimum at  $\lambda = 198$  nm, it appears that the peptide in both the environments predominantly populates unordered conformations, with some significant contribution from antiparallel  $\beta$ -sheets (Table 2). In Figure 3, we reported, for comparison, the CD spectra of CIGB552 and CIGB552TF at 22.3- and 44.6- $\mu\text{M}$  peptide concentrations. These results indicate that the conformational landscape of CIGB552 in the two environments is essentially the same, as proved by the secondary structure analysis of the CD spectra of CIGB552TF reported in Table 3. Unfortunately, this analysis cannot be extended to the higher CIGB552 concentrations investigated by UV-Vis and fluorescence

spectroscopies, due to extensive overlap of CD signals from the chiral excipients in the therapeutic formulation.

### 3.4 | Atomic force microscopy

AFM experiments carried out on peptide films obtained by deposition and overnight drying of CIGB522 and CIGB522TF millimolar solutions on mica revealed interesting differences in the morphologies of the aggregates formed on the solid substrate. In particular, AFM imaging of CIGB552TF showed nanostructures of globular morphology typical of an aggregation process driven by hydrophobic effects (Figure 4A).<sup>28</sup> These globular structures are characterized by a relatively large size distribution, with diameters ranging from 10 to 50 nm. The importance of hydrophobic effects is emphasized by the AFM image reported in Figure 4B, in which the peptide was seen to form, in some limited regions of the mica surface, micrometric annular structures, characterized by an outer diameter of  $990 \pm 10$  nm and an inner diameter of  $56 \pm 9$  nm.<sup>29</sup>

Interestingly, AFM imaging of CIGB552, obtained from deposition of peptide aqueous solutions, (Figure 5) revealed the formation of fibrillar structures, characterized by nanometric lengths ( $377 \pm 112$  nm), and thicknesses ( $26 \pm 6$  nm).

The structures reported in Figure 5B highlights the mechanism of formation of fibrillar aggregates, involving the coalescence and directional growth of nanosized elongated peptide clusters. It has been shown that the formation of such structures is favoured when directional interactions, like hydrogen bonding and  $\pi$ - $\pi$  stacking of aromatic groups, predominate with respect to nonspecific driving forces, like entropically-driven hydrophobic effects.<sup>30</sup> The AFM images reported

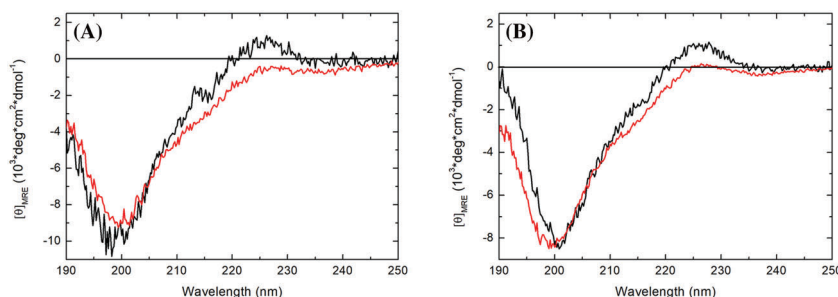
**TABLE 2** Secondary structures adopted by CIGB552 at variable micromolar concentrations in water from circular dichroism experiments

Secondary structure	11.1 $\mu\text{M}$	22.3 $\mu\text{M}$	44.6 $\mu\text{M}$	89.4 $\mu\text{M}$
Coil	45	47	48	54
$\beta$ -sheet (antiparallel)	25	31	35	31
Turn	15	14	13	15
$\beta$ -sheet (parallel)	7	4	3	0
Helix	8	3	0	0

**TABLE 3** Secondary structures adopted by CIGB552 at variable micromolar concentrations in the therapeutic formulation (CIGB552TF) from circular dichroism experiments

Secondary Structure	11.1 $\mu\text{M}$	22.3 $\mu\text{M}$	44.6 $\mu\text{M}$	89.4 $\mu\text{M}$
Coil	49	48	49	55
$\beta$ -sheet (antiparallel)	35	38	38	30
Turn	13	13	13	15
$\beta$ -sheet (parallel)	3	2	0	0
Helix	0	0	0	0

**FIGURE 3** CD spectra of CIGB552 (black) and CIGB552TF (red) at 22.3  $\mu\text{M}$  (A) and 44.6  $\mu\text{M}$  (B) concentrations in water and therapeutic formulation, respectively



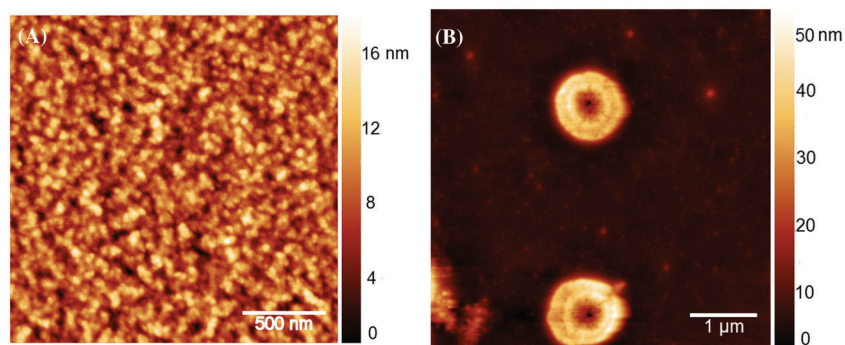


**FIGURE 4** Atomic force microscopy (AFM) images of 1-mM CIGB552TF (therapeutic formulation) aqueous solutions deposited by drop casting and incubated on mica for 18 hours. The images reported in the Figure 4A,B were taken on different areas of the mica surface

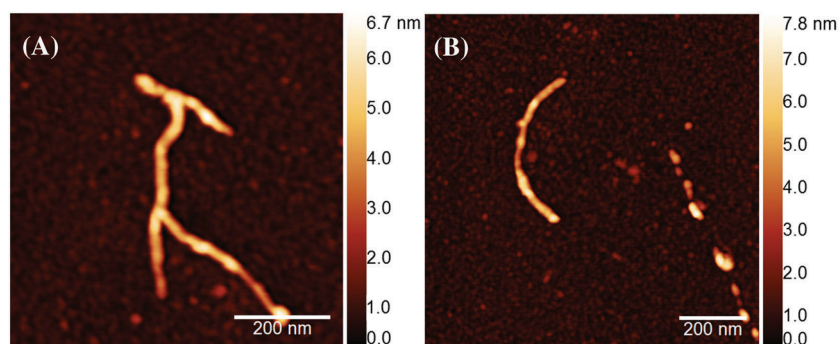


**FIGURE 5** Atomic force microscopy (AFM) images of 1-mM CIGB552 aqueous solutions deposited on mica. Figure 5B clearly shows the alignment of the transient globular structures nucleating the growth of peptide fibrils

in Figure 5 clearly spotted nanometric globules coalescing in fibrillar structures of micrometric length, in close analogy with the formation mechanism of peptide amyloids responsible for several neurodegenerative diseases.<sup>31</sup>

These results clearly agree with the idea that in the therapeutic formulation CIGB552 is well dispersed within the  $\alpha,\alpha$ -trehalose and (L)-tartaric acid matrix, in agreement with spectroscopic results. In contrast, the fibril structures imaged by AFM experiments on CIGB552 deposited on mica from aqueous solutions could be formed only by closely interacting peptide chains, that was only possible in the aqueous peptide formulation.

### 3.5 | Molecular dynamics

#### 3.5.1 | CIGB552 monomer

MD simulations were first carried out for a CIGB552 monomer in 150-mM NaCl aqueous solutions (MD1A), with the aim to mimic physiological conditions, in water (MD1B), to analyse the role of hydrophobic effect, and in an environment mimicking therapeutic formulation (MD1C).

RMSD-based cluster analyses (CA) on MD1A provided for the CIGB552 monomer two predominant cluster-averaged structures, the most representative of which are shown in Figure 6. These clusters account for 51.5% and 28.6% of all sampled conformations, respectively. Interestingly, in the most abundant conformer (Figure 6A), the 20-mer peptide folds into a rather compact structure, characterized by the presence of two antiparallel  $\beta$ -sheet segments.

Centre-of-mass distance distribution analysis revealed that for more than 30% of the sampled conformations, W13 indole and R9 guanidinium are located less than 5 Å away, suggesting the occurrence of a cation- $\pi$  interaction between the two sidechain groups (Figure S12).<sup>32</sup> This finding is confirmed by the analysis of the relative solvent accessibility area (RSA),<sup>25</sup> which drastically decreases to 40% of the maximum allowed accessible surface for the aforementioned residues. This interaction may contribute to stabilize the rather compact structure of conformer A, and it could explain the observed Trp red-shifted emission typical of a polar environment.<sup>33</sup>

Analysis of the distances between the Y15-W13 and Y15-W20 sidechains in MD1A (Figure S13) reveals that for 80% of the former and 70% of the latter pair, the phenol/indole separation distances are definitely shorter than their characteristic Förster distance (9–16 Å). This finding is in close agreement with the fluorescence results reported above, showing an almost complete Tyr  $\rightarrow$  Trp Energy Transfer.

MD simulations of a CIGB552 monomer have also been carried out in the presence of  $\alpha,\alpha$ -threolose and tartaric acid (MD1C) to mimic therapeutic formulation conditions (Table 1). As shown in Figure 7A,  $\alpha,\alpha$ -threolose and tartaric acid molecules bind preferentially to the outer surface of CIGB552, embedding Phe8 in a water-excluded cavity. MD results also indicate that specific interactions involving the  $\alpha,\alpha$ -threolose oxygen atoms and the positively charged Lys5, Lys11 and Lys14 sidechains take place (Figure 7B). These findings are corroborated by the analysis of the solvent accessible surface area of CIGB552, that, in the presence of excipients, decreases by some 40%, involving in particular Phe8 (–79%), Lys12 (–54%), Lys14 (–68%) and Lys18 (–59%).

**FIGURE 6** Most representative structures of CIGB552 from cluster analysis (0.2 nm cut-off) of MD1A simulations in NaCl aqueous solution. Abundances: 51.5% (A); 28.6% (B). The backbone is reported as a ribbon, with the  $\beta$ -sheet tracts coloured in yellow. The side chains of Arg, Trp and Tyr residues are reported as sticks coloured in blue, lime and orange, respectively. A cation- $\pi$  interaction between R9 and W13 can be clearly spotted in the most abundant conformer A

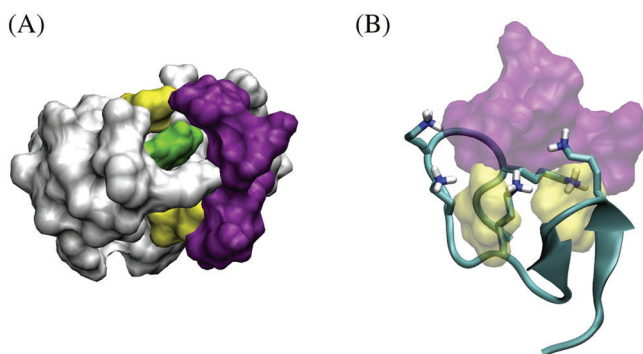
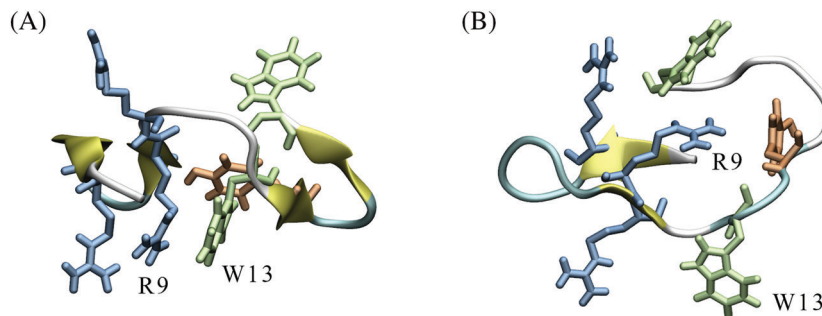


**FIGURE 7** Most representative structure of CIGB552 in the therapeutic formulation from MD1C simulation (600 ns). (A) Surface representation of CIGB552 (white volumes, Phe8 in green), tartaric acid (yellow),  $\alpha,\alpha$ -threulose (violet). (B) Ribbon representation of CIGB552. Tartaric acid and  $\alpha,\alpha$ -threulose are represented as yellow and violet surfaces, respectively (transparency applied)

Energetic analysis carried out on MD1BA and MD1BC reveals the predominant contribution of electrostatic interactions in the stabilization of CIGB552 in the therapeutic formulation environment ( $-10,390 \text{ kJ mol}^{-1}$ ) with respect to the physiological conditions ( $-4750 \text{ kJ mol}^{-1}$ ), matched by a smaller increase of the Van der Waals contributions [ $-539 (\pm 5)$  vs.  $-467 (\pm 4) \text{ kJ mol}^{-1}$ ], in agreement with the results reported in Figure 7B. Overall, these findings strongly suggest that the  $\alpha,\alpha$ -threulose and tartaric acid excipients envelope CIGB552 in a protective shell, inhibiting its aggregation.

### 3.5.2 | CIGB552 aggregates

Aggregation of CIGB552 was studied by MD simulations in a 150-mM NaCl solution (MD4A). To analyze the importance of hydrophobic effects, MD simulations were also carried out under very low ionic conditions (MD4B), as detailed in Table 1. Using the same procedure applied for MD1A, three 200 ns-long trajectories of MD4A were joined and considered as a whole. The obtained ensemble was first analyzed to investigate on the CIGB552 aggregation propensity. In Table 4, the frequency distribution of CIGB552 oligomers is reported, in terms of both the oligomer occurrence and the probability of a single peptide unit to be part of a given oligomer. The results of MD simulation in water (MD4B) are also reported in Table 4 for comparison.

**TABLE 4** CIGB552 oligomer and peptide distribution from MD4 simulation in NaCl 150 mM (MD4A) and in water (low ionic strength) (MD4B)

Oligomer	Oligomer occurrence (%)		Peptide probability (%)	
	MD4A	MD4B	MD4A	MD4B
Monomer	34.8	47.1	16.3	25.6
Dimer	30.1	23.2	28.2	25.3
Trimer	22.1	28.7	31.3	46.9
Tetramer	13.0	1.0	24.4	2.2

From these data, it appears that the formation of peptide oligomers in NaCl is predominant with respect to the presence of monomeric species, indicating a net propensity of CIGB552 to form small peptide clusters in this environment. Interestingly, while in MD4A the monomer/oligomers ratio amounts to 1:2, with a remarkable presence of tetramers, MD4B results show a comparable monomer/oligomer proportion, and a negligible content of tetrameric structures (Figure S4). This finding suggests that hydrophobic effects, notoriously enhanced with increasing the ionic strength, are important for CIGB552 aggregation. In agreement with these considerations, RSA analysis showed that, in the tetramer, the solvent accessibility sensibly decreased in the peptide regions rich of apolar and aromatic residues. In particular, the solvent accessibility of the residues Ile4, Tyr15, Gly17, Phe19 and Trp20 decreases by more than 30% (max 68% in the case of Phe19) in all the four peptides forming the predominant cluster of the tetramer aggregate provided by MD4A (Table S1).

The secondary structure content of the CIGB552 monomer (MD1A, MD1B, MD1C) and tetramer (extracted from MD4A and MD4B) was analyzed by the DSSP algorithm.<sup>25</sup> In all MD simulations CIGB552 populates a rich variety of secondary structures, the abundances of which are summarized in Table 5. From these data, it appears that the conformational landscape of CIGB552 in NaCl is essentially the same in the monomeric and tetrameric structures, with a slight increase of coil and  $\beta$ -sheet conformations at expenses of decreasing bend and turn conformations in the tetrameric structures. As regards the secondary structure content, no significant differences were found for both monomeric and tetrameric species between MD simulations carried out in NaCl and in water.

It should be noted that, although helical conformations are sometimes evocated as intermediates in the self-assembly early stages of



Secondary Structure	MD1A (%)	MD1B (%)	MD1C(%)	MD4A (%)	MD4B (%)
Coil	39	42	48	43	42
$\beta$ -Sheet	20	16	7	21	20
$\beta$ -Bridge	4	4	4	6	3
Bend	23	28	31	19	22
Turn	13	10	9	9	12

**TABLE 5** Secondary structures adopted by CIGB552 from 600 ns MD simulations in 150mM NaCl (MD1A, MD4A), in therapeutic formulation (MD1C) and in water (MD1B, MD4B)

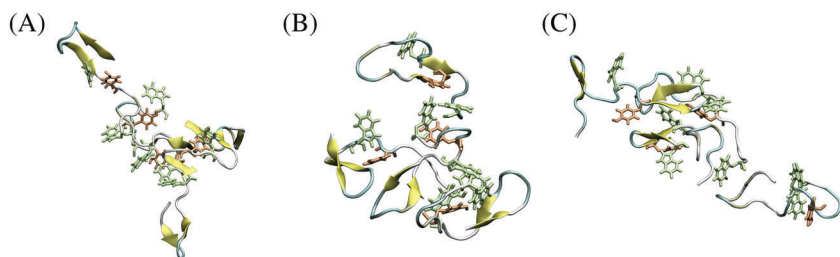


**FIGURE 8** Cluster average structures of CIGB552 tetramers from MD4A simulation in 150 mM NaCl. Abundances: 34.5% (A); 28.7% (B); 22.2% (C). Backbone: ribbon ( $\beta$ -sheet tracts in yellow.); Arg: blue; Trp: lime; Tyr: orange

amyloid fibrils,<sup>34</sup> our analysis does not reveal the presence of helical structures in both CIGB552 monomers and tetramers, suggesting that these conformations do not play a significant role in the aggregation mechanism of this peptide. This finding is supported by CD results, showing that helical secondary structures are definitely minor in water, as well as in the therapeutic formulation.

Cluster analysis of the tetrameric structures extracted from the whole MD4A sampling time, applying the same similarity conditions used for MD1A (0.2-nm cut-off), provided three predominant cluster-averaged structures of comparable abundance, that is, 34.5%, 28.7% and 22.2%, respectively, the most representative of which are shown in Figure 8.

Figure 8 clearly reveals the presence of stretched peptide aggregates, even if more compact configurations also appear with comparable proportion (Figure 8B). At a glance, the interaction between the  $\beta$ -sheet tracts seem to play an important role in the stabilization of the aggregate.

This finding is supported by the energetic analysis of the aggregation process. Actually, the tetramer structure is characterized by large intrapeptide energy contributions, comprising predominant electrostatic ( $4710 \text{ kJ mol}^{-1}$ ) and definitely minor Van der Waals ( $430 \text{ kJ mol}^{-1}$ ) terms. On the contrary, energetic analysis of the tetramer shows comparable interpeptide electrostatic ( $-50 \text{ kJ mol}^{-1}$ ) and Van der Waals ( $-80 \text{ kJ mol}^{-1}$ ) contributions, emphasizing the role of the interaction between non polar residues in the stabilization of the aggregate.

In this regard, one might ask about the role of  $\pi$ - $\pi$  interactions among the four Tyr and eight Trp residues in the stabilization of CIGB552 tetramers. In Figure 9 we reported the separation distance distribution obtained by summing over the 32 Tyr-Trp pair distances for all the tetramers, showing up during the MD4A simulation time.

Similar to MD1A (Figure S3), two well-defined peaks at 6 and 9 Å, respectively, fall well below the Tyr-Trp Förster distance, accounting for the very efficient energy transfer observed at all the peptide concentrations investigated. Interestingly, the maxima of the Tyr-Trp

distance distribution are regularly spaced by 4 Å, a typical distance between aromatic groups stabilized by stacking interactions.<sup>35</sup> The observed regularity of the separation patterns extends over distances longer than 2 nm, a clear indication of the stability of tetrameric structures.

In Figures 9, we partitioned the distance distribution between intra- and inter-peptide Tyr-Trp pairs in the tetrameric structures. This partition shows that distances comprised within 1 nm are mostly accounted for by intra-peptide interactions, and are almost absent in the inter-strand component of the distance distribution. These data strongly suggest that  $\pi$ - $\pi$  interactions stabilize the single chain conformation in the oligomers but do not contribute to the inter-peptide interactions.

This conclusion is strengthened by taking into account the 6 Tyr-Tyr (Figure S15) and 56 Trp-Trp (Figure S6) distance distributions. The former represents a topological parameter that depends only on inter-peptide interactions. In this case, a regular pattern of distances was observed (Figure S5), characterized by two distribution peaks centred at around 1.3 and 1.8 nm, and the absence of short distances contributions. The same pattern was observed for both the intra- and inter-strand contributions to the Trp-Trp distance distribution.

Well-ordered aggregates forms also if inter-peptide  $\pi$ - $\pi$  interactions seem to play a minor role. To investigate the inter-molecular interactions on the basis of the observed order, we have analyzed the hydrogen bonding (HB) network in the CIGB552 tetramer. Where the HB connectivity map is considered, three very stable (30%–50% of the simulation time) and a dozen of quite stable (10%–30% of the simulation time) inter-peptide HB contacts have found to stabilize the peptide tetramer (Figure S7).

Overall, these findings suggest that aromatic-aromatic interactions are important to stabilize the secondary structure ordering of the single peptide units, that form relatively stable oligomers, maintained by hydrophobic interactions and by a long-lasting inter-peptide HB network.

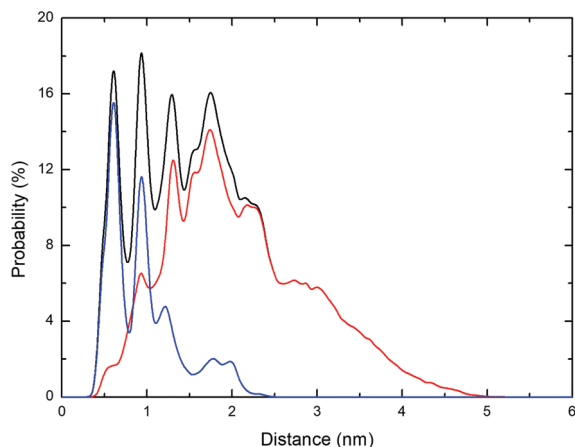


**FIGURE 9** Distance distribution of Tyr-Trp pairs in the tetrameric structures from MD4A simulation. (A) Black: sum over all 32 Tyr-Trp distances; blue: Intra-peptide distance distribution; red: Inter-peptide distance distribution

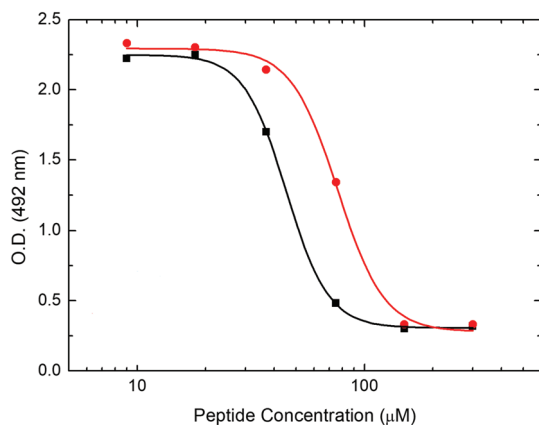


**FIGURE 10** Cell viability assay of CIGB522 (red dots and line) and CIGB522TF (black squares and line) on H-460 cell line. The optical density of sulforhodamine B at  $\lambda = 492$  nm was reported as a function of the peptide micromolar concentration (log scale)

**TABLE 6** Effect of the peptide therapeutic formulation (CIGB522TF) and aqueous solution (CIGB522) on the cell viability in H-460 tumour cell line

	CIGB522TF	CIGB522
H-460 IC <sub>50</sub> ( $\mu$ Mol/L) <sup>a</sup>	58 $\pm$ 3	94 $\pm$ 11

<sup>a</sup>Mean  $\pm$  SD of three determinations on three different peptide lots.

Interestingly, in all the structures reported in Figures 6 and 8, most of the charged peptide side-chains (i.e., the four Lys and three Arg residues) protrude outwards into the solvent, providing the peptide surface of a net positive charge character. These residues represent the most suitable sites for interacting with the  $\alpha,\alpha$ -threosyl oxygen atoms, as clearly shown by MD1C results (Figure 7). This

finding may also explain for the strong cell-penetrating properties of CIGB522 in its monomeric form, as well as small peptide oligomers.

### 3.6 | Cell viability assay

In order to study the cytotoxic activity of the investigated peptide in aqueous solution and in its therapeutic formulation, a cell viability assay was performed on H-460 cell line. IC<sub>50</sub> values were obtained by fitting the experimental data, that is, the optical densities (OD) of sulforhodamine B at  $\lambda = 492$  nm at different peptide concentration, by the Hill equation<sup>36</sup>:

$$OD(x) = OD_{\max} \frac{OD_{\max} - OD_{\min}}{1 + \left(\frac{x}{IC_{50}}\right)^H}$$

where  $x$  represents the peptide concentration and  $H$  the phenomenological Hill number. Figure 10 shows the result of a typical experiment of cell viability assay for the two peptide formulations investigated.

Interestingly, CIGB522TF shows IC<sub>50</sub> values definitely lower than the aqueous peptide formulation (Table 6). This result strengthens the idea that the formulation of the peptide, and therefore its aggregation state, is relevant for its biological activity.

## 4 | CONCLUSIONS

The aggregation properties of CIGB522 in water and in its therapeutic formulation were investigated by optical spectroscopy and microscopy technique with nanometric resolution. UV-Vis and fluorescence experiments showed that the excipients, that is, 50.7%  $\alpha,\alpha$ -trehalose, and 17.2% (L)-tartaric acid, strongly deplete the peptide aggregation propensity in the therapeutic formulation, maintaining the peptide in its monomeric form. MD simulations carried out on the CIGB522/ $\alpha,\alpha$ -trehalose/(L)-tartaric acid system, showed that the excipients strongly bind to the charged Lys and Arg residues, involved in the H-bond network stabilizing the aggregate, forming a protective shell that weakens the inter-molecular interactions, and in turn decreases the stability of the peptide aggregates. This finding is strengthened by AFM experiments that showed that the peptide in its therapeutic formulation formed almost exclusively globular aggregates, a morphology typical of aggregation processes driven by hydrophobic effect.

The role of hydrophobic effects was highlighted by the comparison of MD simulations carried out in water and under ionic strength conditions mimicking physiological conditions. In particular, AFM imaging revealed the fibrillization of aggregates formed from deposition of aqueous CIGB522 solution. In this regard, it is important to stress that formation of peptide fibrils necessitates of specific peptide-peptide interaction.<sup>37,38</sup> MD simulations suggest that an inter-strand HB network concurs to stabilize peptide clusters, and

these interactions could be the basis of the clear directionality observed in the formation of fibrillar aggregates from the coalescence of globular structures.

All these findings strongly suggest that trehalose-CIGB552 interactions may take place in the therapeutic formulation, inhibiting peptide fibrillogenesis. Trehalose-peptide conjugates have already been shown to act as inhibitors of amyloid fibrillation,<sup>39</sup> enhancers of resistance towards proteolytic degradation,<sup>40</sup> and protectants against thermal denaturation of proteins.<sup>41</sup>

These ideas pave the way for explaining the higher cytotoxic activity of CIGB552 in its therapeutic formulation, suggesting that peptide fibrillation may inhibit its therapeutic activity. On the other hand, control of the morphology of peptide nanostructures could represent a suitable approach for modulating the efficiency of therapeutic peptides through fine tuning of their pharmacokinetics.<sup>42</sup>

## ACKNOWLEDGEMENTS

This project received funding from the European Union Horizon 2020 Research and Innovation Program under the H2020 Marie Skłodowska-Curie Actions grant agreement no. 872233 ("PEPSA-MATE"). GB acknowledge CINECA and the EU-PRACE programme for the CPU time.

## ORCID

Mariano Venanzi  <https://orcid.org/0000-0001-9364-7441>

## REFERENCES

1. Malonis RJ, Lai JR, Vergnolle O. Peptide-based vaccines: current progress and future challenges. *Chem Rev*. 2020;120:3210-3229. <https://doi.org/10.1021/acs.chemrev.9b00472>
2. Vlieghe P, Lisowski V, Martinez J, Khrestchatskiy M. Synthetic therapeutic peptides: science and market. *Drug Discov Today*. 2010;15:40-56. <https://doi.org/10.1016/j.drudis.2009.10.009>
3. Blanco-Míguez A, Gutiérrez-Jácome A, Pérez-Pérez M, et al. From amino acid sequence to bioactivity: the biomedical potential of antitumor peptides. *Protein Sci*. 2016;25:1084-1095. <https://doi.org/10.1002/pro.2927>
4. Albericio F, Kruger HG. Therapeutic peptides. *Future Med Chem*. 2012;4:1527-1531. <https://doi.org/10.4155/fmc.12.94>
5. Wu D, Gao Y, Qi Y, Chen L, Ma Y, Li Y. Peptide-based cancer therapy: opportunity and challenge. *Cancer Lett*. 2014;35:13-22. <https://doi.org/10.1016/j.canlet.2014.05.002>
6. Thundimadathil J. Cancer treatment using peptides: current therapies and future prospects. *J Amino Acids*. 2012; 967347. <https://doi.org/10.1155/2012/967347>
7. Vallespi MG, Fernandez JR, Torrens I, et al. Identification of a novel antitumor peptide based on the screening of an Ala-Library derived from the LALF(32-51) region. *J Pept Sci*. 2010;16:40-47. <https://doi.org/10.1002/psc.1192>
8. Massó JRF, Oliva Argüelles B, Tejada Y, et al. The antitumor peptide CIGB-552 increases COMMD1 and inhibits growth of human lung cancer cells. *J Amino Acids*. 2013; 251398. <https://doi.org/10.1155/2013/251398>
9. Vallespi MG, Pimentel G, Cabrales-Rico A, et al. Antitumor efficacy, pharmacokinetic and biodistribution studies of the anticancer peptide CIGB-552 in mouse models. *J Pept Sci*. 2014;20:850-859. <https://doi.org/10.1002/psc.2676>
10. Vallespi MG, Rodriguez JC, Seoane LC, et al. The first report of cases of pet dogs with naturally occurring cancer treated with the antitumor peptide CIGB-552. *Res Vet Sci*. 2017;114:502-510. <https://doi.org/10.1016/j.rvsc.2017.09.029>
11. Burstein E, Hoberg JE, Wilkinson AS, et al. COMMD proteins, a novel family of structural and functional homologs of MURR1. *J Biol Chem*. 2005;280:22222-22232. <https://doi.org/10.1074/jbc.M501928200>
12. van de Sluis B, Mao X, Zhai Y, et al. COMMD1 disrupts HIF-1alpha/beta dimerization and inhibits human tumor cell invasion. *J Clin Invest*. 2010;120:2119-2130. <https://doi.org/10.1172/JCI40583>
13. Nunez de Villavicencio-Diaz T, Ramos Gomez Y, Oliva Argüelles B, et al. Comparative proteomics analysis of the antitumor effect of CIGB-552 peptide in HT-29 colon adenocarcinoma cells. *J Proteomics*. 2015;126:163-171. <https://doi.org/10.1016/j.jprot.2015.05.024>
14. Rodriguez-Ulloa A, Gil J, Ramos Y, et al. Proteomic study to survey the CIGB-552 antitumor effect. *Biomed Res Int*. 2015; 124082. <https://doi.org/10.1155/2015/124082>
15. Daghero H, Fernández Massó JR, Astrada S, Guerra-Vallespi MG, Bollati-Fogolin M. The anticancer peptide CIGB-552 exerts anti-inflammatory and anti-angiogenic effects through COMMD1. *Molecules*. 2021;26:152. <https://doi.org/10.3390/molecules26010152>
16. Micsonai A, Wien F, Kernya L, et al. Accurate secondary structure prediction and fold recognition for circular dichroism spectroscopy. *Proc Natl Acad Sci USA*. 2015;E3095-E3103. <https://doi.org/10.1073/pnas.1500851112>
17. Berendsen HJC, van der Spoel D, van Drunen R. GROMACS: a message-passing parallel molecular dynamics implementation. *Comput Phys Commun*. 1995;91:43-56. [https://doi.org/10.1016/0010-4655\(95\)00042-E](https://doi.org/10.1016/0010-4655(95)00042-E)
18. Oostenbrink C, Villa A, Mark AE, van Gunsteren WF. A biomolecular force field based on the free enthalpy of hydration and solvation: the GROMOS force-field parameter sets 53A5 and 53A6. *J Comput Chem*. 2004;25:1656-1676. <https://doi.org/10.1002/jcc.20090>
19. Bussi G, Donadio D, Parrinello M. Canonical sampling through velocity rescaling. *J Chem Phys*. 2007;126: 014101. <https://doi.org/10.1063/1.2408420>
20. Malde AK, Zuo L, Breeze M, et al. An Automated force field Topology Builder (ATB) and repository: version 1.0. *J Chem Theory Comput*. 2011;7:4026-4037. <https://doi.org/10.1021/ct200196m>
21. Stroet M, Caron B, Visscher K, Geerke D, Malde AK, Mark AE. Automated topology builder version 3.0: prediction of solvation free enthalpies in water and hexane. *J Chem Theory Comput*. 2018;14(11): 5834-5845. <https://doi.org/10.1021/acs.jctc.8b00768>
22. Parrinello M, Rahman A. Polymorphic transitions in single crystals: a new molecular dynamics method. *J Appl Phys*. 1981;52:7182-7190. <https://doi.org/10.1063/1.328693>
23. Darden T, York D, Pedersen L. Particle mesh Ewald: an N-log(N) method for Ewald sums in large systems. *J Chem Phys*. 1993;98: 10089-11092. <https://doi.org/10.1063/1.464397>
24. Humphrey W, Dalke A, Schulten K. VMD: visual molecular dynamics. *J Mol Graph*. 1996;14:33-38. [https://doi.org/10.1016/0263-7855\(96\)00018-5](https://doi.org/10.1016/0263-7855(96)00018-5)
25. Tien MZ, Meyer AG, Sydykova DK, Spielman SJ, Wilke CO. Maximum allowed solvent accessibilities of residues in proteins. *PLoS ONE*. 2013;8: e80635. <https://doi.org/10.1371/journal.pone.0080635>
26. Kabsch SC. Dictionary of protein secondary structure: pattern recognition of hydrogen-bonded and geometrical features. *Biopolymers*. 1983;22:2577-2637. <https://doi.org/10.1002/bip.360221211>
27. Daura X, Gademann K, Jaun B, Seebach D, van Gunsteren WF, Mark AE. Peptide folding: when simulation meets experiment. *Angew Chem Int Ed*. 1999;38:236-240. [https://doi.org/10.1002/\(SICI\)1521-3773\(19990115\)38:236::AID-ANGE236>3.0.CO;2-1](https://doi.org/10.1002/(SICI)1521-3773(19990115)38:236::AID-ANGE236>3.0.CO;2-1)
28. Caruso M, Placidi E, Gatto E, et al. Fibers or globules? Tuning the morphology of peptide aggregates from helical building blocks. *J Phys Chem B*. 2013;117:5448-5459. <https://doi.org/10.1021/jp400009j>

29. Caruso M, Gatto E, Placidi E, et al. A single-residue substitution inhibits fibrillization of Ala-based pentapeptides. A spectroscopic and molecular dynamics investigation. *Soft Matter*. 2014;10:2508-2519. <https://doi.org/10.1039/C3SM52831F>
30. De Zotti M, Muzzi B, Gatto E, et al. Tuning the morphology of nanostructured peptide films by the introduction of a secondary structure conformational constraint: a case study of hierarchical self-assembly. *J Phys Chem B*. 2018;122:6305-6313. <https://doi.org/10.1021/acs.jpcc.8b01877>
31. Luo J, Wärmländer SKTS, Gräslund A, Abrahams JP. Alzheimer peptides aggregates into transient nanoglobules that nucleate fibrils. *Biochemistry*. 2014;53:6302-6308. <https://doi.org/10.1021/bi5003579>
32. Gallivan JP, Dougherty DA. Cation- $\pi$  interactions in structural biology. *Proc Natl Acad Sci USA*. 1999;96:9459-9464. <https://doi.org/10.1073/pnas.96.17.9459>
33. Hamm HE, Meier SM, Liao G, Preininger AM. Trp fluorescence reveals an activation-dependent cation- $\pi$  interaction in the switch II region of  $G\alpha_i$  proteins. *Protein Sci*. 2009;18:2326-2335. <https://doi.org/10.1002/pro.243>
34. Abedini A, Raleigh DP. A role for helical intermediates in amyloid formation by natively unfolded polypeptides? *Phys Biol*. 2009;6: 015005. <https://doi.org/10.1088/1478-3975/6/1/015005>
35. Chelli R, Gervasio FL, Procacci L, Schettino V. Stacking and T-Shape competition in aromatic-aromatic amino acid interaction. *J Am Chem Soc*. 2002;124:6133-6143. <https://doi.org/10.1021/ja0121639>
36. Beam A, Motsinger-Reif A. Beyond IC50s: Towards Robust Statistical Methods for in vitro Association Studies. *J Pharmacogenomics Pharmacoproteomics*. 2014;5: 1000121. <https://doi.org/10.4172/2153-0645.1000121>
37. Hamley IW. Peptide fibrillization. *Angew Chem Int Ed*. 2007;46: 8128-8147. <https://doi.org/10.1002/anie.200700861>
38. Venanzi M, Savioli M, Cimino R, et al. A spectroscopic and molecular dynamics study on the aggregation process of a long-acting lipidated therapeutic peptide: the case of semaglutide. *Soft Matter*. 2020;16: 10122-10131. <https://doi.org/10.1039/D0SM01011A>
39. De Bona P, Giuffrida ML, Caraci F, et al. Design and synthesis of new trehalose-conjugated pentapeptides as inhibitors of  $A\beta(1-42)$  fibrillogenesis and toxicity. *J Pept Sci*. 2009;15:220-228. <https://doi.org/10.1002/psc.1109>
40. Di Natale G, Zimbone S, Bellia F, Giuffrida ML, Pappalardo G, Rizzarelli E. Potential therapeutics of Alzheimer's diseases: New insights into the neuroprotective role of trehalose-conjugated beta sheet breaker peptides. *Peptide Science*. 2018;110: e24083. <https://doi.org/10.1002/psc.1109>
41. Paul S, Paul S. Molecular insights into the role of aqueous trehalose solution on temperature-induced protein denaturation. *J Phys Chem B*. 2015;119:1598-1610. <https://doi.org/10.1021/jp510423n>
42. Gerbelli BB, Vassiliades SV, Rojas JEU, et al. Hierarchical self-assembly of peptides and its applications in bionanotechnology. *Macromol Chem Phys*. 2019;220: 1900085. <https://doi.org/10.1002/macp.201900085>

### SUPPORTING INFORMATION

Additional supporting information may be found online in the Supporting Information section at the end of this article.

**How to cite this article:** Savioli M, Antonelli L, Bocchinfuso G, et al. Formulation matters! A spectroscopic and molecular dynamics investigation on the peptide CIGB552 as itself and in its therapeutical formulation. *J Pep Sci*. 2021;e3356. <https://doi.org/10.1002/psc.3356>